sciendo

POLISH MARITIME RESEARCH 4 (100) 2018 Vol. 25; pp. 83-97
10.2478/pomr-2018-0135

DYNAMIC ANALYSIS OF EMBEDDED CHAINS IN MOORING LINE FOR FISH CAGE SYSTEM

Hui-Min Hou
Guo-Hai Dong
Tiao-Jian Xu
Yun-Peng Zhao
Chun-Wei Bi
State Key Laboratory of Coastal and Offshore Engineering, Dalian University of Technology, China

ABSTRACT

Investigation of the embedded chains in soil starts to play an important role in understanding the structural performance of mooring system, when the embedded anchors will be employed to sustain large loads with the gradually growth of installation depth of offshore aquaculture farm. The aim of this study is to investigate the dynamic response of mooring line considering the influence of embedded chains in clay soil for net cage system. Lumped-mass method is used to establish the numerical model for evaluating the performance of mooring line with embedded chains. To validate the numerical model, comparisons of numerical results with the analytical formulas and the experimental data are conducted. A good agreement of the profile and the tension response is obtained. Then, the effect of embedded chains on the static and dynamic response of mooring line is evaluated, and the dynamic behavior of mooring system considering embedded chains for net cage system is investigated. The results indicate that the soil resistance on embedded chains should be included to predict the mooring line development and the load on the embedded anchors in the numerical simulations. An appropriate safety factor should be included if employing the simplified model Case C at the initial design phase. And the effect of embedded chains on the holding capacity of embedded anchors in single-point mooring system for single net cage cannot be negligible during the design and operation phases. Consequently, it is profound to take into account the interaction of embedded chains and soil for accurately predicting the reliability of mooring system for fish cage.

Keywords: embedded chains, soil resistance, parameter sensitivity, dynamic analysis

INTRODUCTION

According to Kapetsky et al. 2013, the potential of the offshore aquaculture is large due to the inshore space competition, wave quality problems, food security concern and environmental and aesthetic impacts. For the fish farm installed in the open sea, the mooring system should be re-designed since the load is more severe than that for the inshore fish farm. Similar to the offshore drilling platform, suction anchors may be employed in mooring system of offshore fish farm due to the advantage of simple design, high resistance against vertical loading, simple and fast installation (Cheng et al. 2014). Generally, the attachment point of suction anchors is below the seabed level and the chains are employed to avoid the abrasion and wear when the interaction between mooring line and the seabed occurs. Thus, it is essential to consider the interaction of embedded chains and soil to analyze the structural performance of mooring system for fish farm.

Numerous existing researches on the hydrodynamic behavior of mooring system for fish cage were conducted involving physical experiments and numerical models, assuming that the anchor point was fixed at the seabed. Huang et al. 2010 recorded mooring line tension of a single-point-mooring cage system by a full-scale physical model, where a concrete block was used as an anchor. Tang et al. 2011 investigated the dynamic properties of a dual pontoon floating cage structure by physical model, which is moored to the load cells by a symmetric coil spring connected by

rollers fixed to the seabed. Xu et al. 2013 measured the tension forces on the mooring line in submerged mooring grid system of a scaled fish cage model. Zhao et al. 2015 conducted a series of physical model experiments to measure the mooring line tension for multiple net cages in steady current. DeCew et al. 2010 employed a finite element analysis program to predict the tension response of a single-point mooring system under a variety of currents. Shainee et al. 2013 numerically investigated the submergence characteristics of a single-point-mooring fish cage system, considering the mooring line anchored to the seabed directly. Kim et al. 2014 modeled the hydrodynamic response of the moored containment structure using the finite element model. Huang et al. 2016 developed a finite element model to investigate the elastic deformations and mooring line tension of floating collar in waves.

Provided that the embedded anchors would be utilized to sustain larger loads than the dead weight anchors, the mooring system including the chains embedded in soil is becoming more popular when the environmental loading is extremely severe in the open sea. Some researches considering mooring chains embedded in soil have been conducted by laboratory tests and numerical simulations. Choi et al. 2014 conducted the lab-scale model tests to obtain the pullout capacity of embedded chains. O'Loughlin et al. 2015 observed the chain-soil interaction during physical model tests and estimated the capacity of the mooring chain both on and within the seabed. Rocha et al. 2016 performed the physical experiment to investigate the static load attenuation from the soil frictional forces for embedded chains, and then the relationship between mean ratio of the frictional to transversal force and the undrained soil shear strength was studied. Wang et al. 2010a proposed a two-dimensional static model and a three-dimensional quasi-static model to predict the mooring cable behavior considering the currents, soil resistance and cable elasticity during pretensioning and in service. Wang et al. 2010b adopted the three-dimensional numerical model for embedded chains to obtain the chain profiles and tension distributions under different pretension levels. Guo et al. 2016 employed a two-dimensional quasi-static model to predict the response of mooring lines comprising multiple types of mooring lines or chains. Xiong et al. 2016 investigated the influence of embedded chains on the response of mooring line considering the interaction of soil and chains.

However, the understanding of the dynamic response of mooring line considering the effect of embedded chains is still not comprehensive. And with the enormous potential application of the embedded anchors in the open ocean aquaculture industry, the interaction of embedded chains and soil for offshore aquaculture farm needs to make a quantitative estimation. In addition, the safety of the embedded anchors will be of vital importance for the entire system of aquaculture farm since the cost of mooring system with the embedded anchors is high and the installation and maintenance cost increases significantly with the growth of water depth. And in the design of net cage system in the open sea, it is a challenging problem to obtain the most optimized balance between the cost and the safety of embedded anchors including the interaction of embedded chains and soil. Therefore, the importance in modeling embedded chains of mooring line and the parameter sensitivity should be investigated to better understand the structural response of mooring line with embedded chains. And the influence of embedded chains on the dynamic response of offshore fish farm should be evaluated to provide a basis for the design of embedded anchors. In this study, the performance of mooring line including embedded chains is predicted using the lumped-mass method. The effect of embedded chains on the structural response of mooring line is quantified by the proposed numerical model. And the sensitivity of the response of mooring line with embedded chains to the variation of parameters, including initial pretension level of mooring line, soil shear strength gradient and the multipliers in soil resistance, is conducted in static and dynamic analysis. Furthermore, the dynamic response of mooring system for net cage system is investigated considering the effect of embedded chains.

NUMERICAL SIMULATION

To provide a better understanding of the performance of embedded chains in mooring system and help improve the future prediction for the structural response of open sea fish farm, a numerical model for mooring line including embedded chains (as depicted in Fig. 1) is developed based on the lumped mass method in this study.

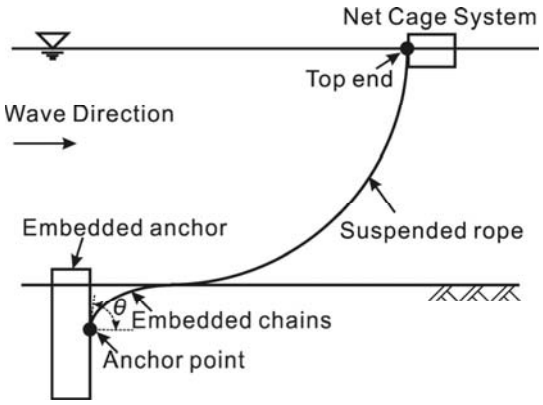

Fig. 1 Definition of the mooring line considering embedded chains

LUMPED MASS MODEL

The lumped mass method is used to model the structural behavior of mooring line with embedded chains. And only tension effect of mooring line is considered ignoring bend and torsion effects and the mooring line is assumed to be anchored to the fixed embedded anchors.

In the proposed numerical model, the entire mooring line is divided into numerous elements to calculate the dynamic behavior of mooring system, as depicted in Fig. 2. An element is composed of two end nodes and a mass-less spring. Mass of each element is concentrated at the end nodes and the mass

nodes are connected by the elastic spring without mass. The tension force at the two ends of each element becomes the concentrated load acting on the corresponding end nodes. And the external forces on each element are calculated first and then evenly distributed to the corresponding end nodes. More details about the lumped mass method can refer to many references, e.g. Huang et al. 2006, Surendran and Goutam 2009, Masciola et al. 2011 and Hall and Goupee 2015).

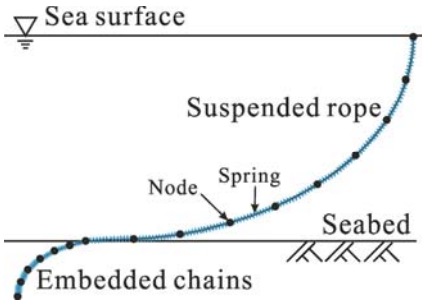

Fig. 2 Schematic of mass-spring model for mooring line

HYDRODYNAMIC LOADS ON MOORING LINE

A local coordinate system (o'-τ-η-ξ) (see Fig. 3) is defined to describe the direction of the hydrodynamic forces acting on elements. Concerning the local coordinate system o'-τ-η-ξ, the η-axis lies on the plane that includes the τ-axis and *V*, and the velocity vector of the water particle at the mid-point of the element can be divided into τ (tangential) and η (normal) components. The scattering effect of the net twine on the flow field can be neglected because the diameter of net twine is relatively small compared with the characteristic wave length.

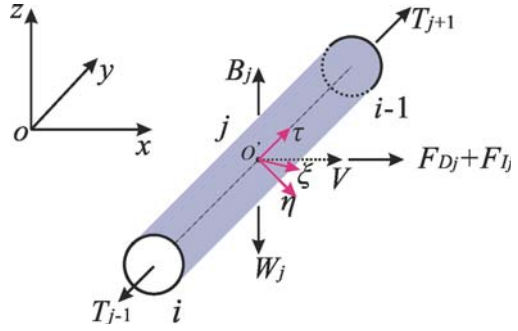

Fig. 3 Schematic of the local coordinate system for an element j of suspended rope

Thus, it is appropriate to calculate the wave loads on the net using the modified Morison equation considering the relative motion between net element and flow field,

$$\begin{cases} F_\tau = \frac{1}{2} C_{D\tau} \rho A_\tau |u_\tau - \dot{R}_\tau| \cdot (u_\tau - \dot{R}_\tau) + \rho V_0 a_\tau + C_{m\tau} \rho V_0 |a_\tau - \ddot{R}_\tau| \\ F_\eta = \frac{1}{2} C_{D\eta} \rho A_\eta |u_\eta - \dot{R}_\eta| \cdot (u_\eta - \dot{R}_\eta) + \rho V_0 a_\eta + C_{m\eta} \rho V_0 |a_\eta - \ddot{R}_\eta| \\ F_\xi = \frac{1}{2} C_{D\xi} \rho A_\xi |u_\xi - \dot{R}_\xi| \cdot (u_\xi - \dot{R}_\xi) + \rho V_0 a_\xi + C_{m\xi} \rho V_0 |a_\xi - \ddot{R}_\xi| \end{cases} \quad (1)$$

where F_η and F_ξ are the normal components of external forces on the net twine, and F_τ is the tangential component of external forces on the net twine; $\vec{u} = (u_\tau, u_\eta, u_\xi)$ is the fluid particle velocity vector at the element center; $\vec{R} = (\dot{R}_\tau, R_\eta, R_\xi)$ is the central velocity vector of element; $\vec{\dot{u}} = (\dot{u}_\tau, \dot{u}_\eta, \dot{u}_\xi)$ is the fluid particle acceleration vector at the element center; $\vec{\ddot{R}} = (\ddot{R}_\tau, \ddot{R}_\eta, \ddot{R}_\xi)$ is the central acceleration vector of element; ρ is the density of water; V_0 is the water displaced volume of an element; A_τ, A_η and A_ξ are the effective projected areas of an element in the direction of the τ, η and ξ components, respectively; $C_{D\tau}$, $C_{D\eta}$ and $C_{D\xi}$ are the drag coefficients in the direction of the τ, η and ξ components, respectively; $C_{m\tau}$, $C_{m\eta}$ and $C_{m\xi}$ are the added mass coefficients in the direction of the τ, η and ξ components, respectively.

For the suspended-part of mooring line in water, the hydrodynamic coefficients are calculated using a method described by Choo and Casarella 1971:

$$C_\eta = \begin{cases} 8\pi/(\mathrm{Re}_\eta \cdot s) \cdot (1 - 0.87 s^{-2}) & (0 < \mathrm{Re}_\eta \le 1) \\ 1.45 + 8.55 \mathrm{Re}_\eta^{-0.90} & (1 < \mathrm{Re}_\eta \le 30) \\ 1.1 + 4 \mathrm{Re}_\eta^{-0.50} & (30 < \mathrm{Re}_\eta \le 10^5) \end{cases} \quad (2)$$

$$C_\tau = \pi \cdot \mu \cdot \left(0.55 \mathrm{Re}_\eta^{1/2} + 0.084 \mathrm{Re}_\eta^{2/3}\right) \quad (3)$$

where $R_{e\eta}=\rho V_{R\eta} D/\mu$; $s=-0.077215665+\ln(8/Re_\eta)$; μ is the viscosity of water; C_η and C_τ are the normal and tangential drag coefficients for mesh bar; $V_{R\eta}$ is the normal component of the fluid velocity relative to the bar; ρ is the density of water and is assumed as 1000 kg/m^3.

SOIL RESISTANCE ON EMBEDDED CHAINS

A segment for embedded chains in clay soil is presented in Fig. 4. The soil resistance consists of two components: the normal resistance *Q* and the tangential resistance *F*.

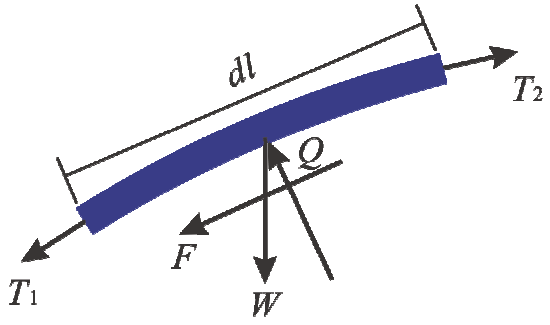

Fig. 4 Force sketch of embedded chains in soil

According to Skempton 1951 and Gault and Cox 1974, the soil resistance per unit length of embedded chains for clay soils can be expressed as,

$$\begin{aligned} Q &= E_n \cdot d \cdot N_c \cdot s_u \\ F &= E_\tau \cdot d \cdot s_u \end{aligned} \quad (4)$$

where E_n and E_τ are the multipliers for the effective width in the normal and tangential directions; *d* is the nominal

diameter of embedded chains; s_u is the undrained shear strength of soil (Yen and Tofani 1984); N_c is a bearing capacity factor and set as 7.6 for simplicity (Skempton 1951, Degenkamp and Dutta 1989). Degenkamp and Dutta 1989 recommended the values of E_n and E_τ for the chains as 2.5 and 8.0, respectively. The undrained soil shear strength is proportional to the embedded depth,

$$s_u = s_{u0} - k \cdot z \tag{5}$$

where s_{u0} is the soil shear strength at the seabed level; k is the soil shear strength gradient; z is the depth measured from the seabed level downwards. In this study, s_{u0} = 0.0 kPa (Neubecker and Randolph 1995, Liu et al. 2014, Xiong et al. 2016, Racha et al. 2016) and k = 1.45 kPa/m (Andersen et al. 2005).

TENSION ON MOORING LINE

The mooring line usually consists of fiber rope and embedded chains. The embedded chain located at the lower part of mooring line is linked to the embedded anchors to avoid the decrease in the strength due to excessive friction with the sea floor. The material of fiber rope is polypropylene (PP) and the material of mooring chains is steel. The elasticity relationship of fiber rope is T=3.52($\Delta S/S$)$^{1.132}$, where T is the tension on fiber rope with the unit of MN; ΔS is the elongation of fiber rope; S is the initial length of fiber rope (referring to Xu 2014). The tension on mooring chains can be calculated through T=284.2($\Delta l/l$), where T is the tension on chains with the unit of MN; Δl is the elongation of chains; l is the initial length of chains.

MOTION EQUATION

The forces on the element are distributed to the end nodes evenly after calculating the hydrodynamic loads, soil resistance and tension force on each element in the local coordinate system, and then the force on the nodes in the local coordinate system are transformed into the global coordinate system. According to the Newton's second law, the motion equation for the lumped mass point is given as

$$M\vec{\ddot{R}} = \vec{T} + \vec{W} + \vec{F}_{envir} \tag{6}$$

where M is the mass of the lumped mass point; $\vec{\ddot{R}}$ is the acceleration vector of the mass center of the lumped mass point; $\vec{T}$ is the elastic tension vector between the lumped mass points; $\vec{W}$ is the gravity force on the lumped mass point; $\vec{F}_{envir}$ is the environmental force acting on the lumped mass point. The environmental force on suspended fiber rope is composed of the drag force, inertia force and buoyant force in water, while the environmental force on embedded chains consists of the soil resistance and the buoyancy force in soil (Degenkamp and Dutta 1989). Runge-Kutta-Verner fifth-order and sixth-order method is adopted to solve the equations. More details about the motion equation of lumped mass points can refer to Xu et al. 2013.

VALIDATION OF THE NUMERICAL MODEL

In order to validate the proposed numerical model, the analytical solutions and the experimental results for investigating the structural response of mooring line from previous researches are compared with the numerical results in static analysis and dynamic analysis, respectively.

STATIC ANALYSIS

The validations are performed for the static response of embedded chains and suspended rope. Referring to Neubecker and Randolph 1995, the analytical form for the profile of embedded chains is written as Eq. (A.3) shown in Appendix A. Fig. 5 presents the profiles of embedded chains for different chain angles θ_o at the seabed obtained from the numerical model and the analytical formulation, where the non-dimensional tension at the anchor point is T^*=4 and T^*=20. A good agreement is obtained, and thus the proposed model is reasonable to calculate the profile and static tension response of embedded chains.

a)

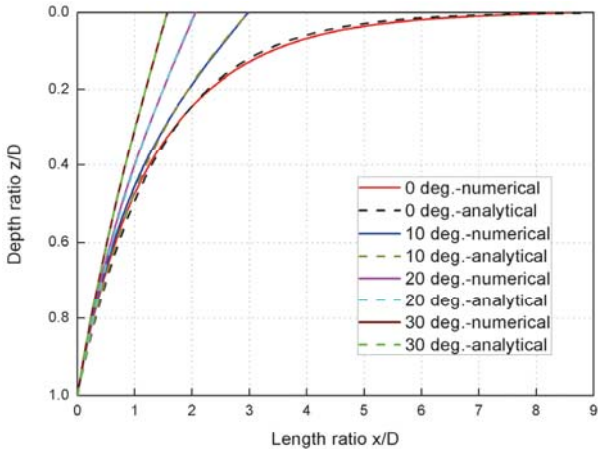

b)

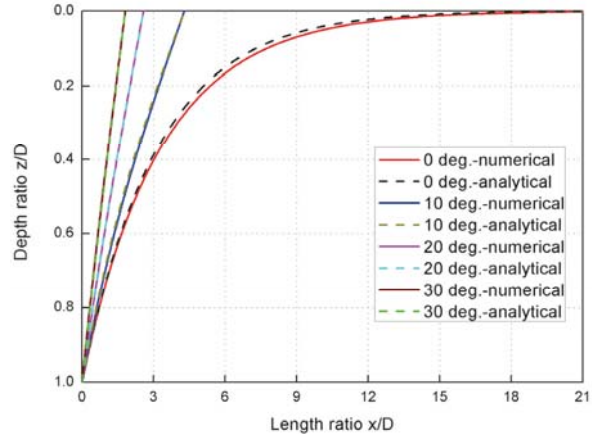

Fig. 5 Profiles of embedded chains for different chain angles at seabed: (a) T^*=4; (b) T^*=20

In addition, the static response of suspended rope is validated by catenary equation when the elongation is insignificant. The sketch of and the force acting on catenary curve is shown in Fig. 6. According to Cella 1999, the analytical form for the static response of catenary curve is listed in Appendix B. The configuration of fiber rope suspended in water can be calculated by Eq. (B.4) and the tension at the top end is obtained by Eq. (B.6). Here, the length of fiber rope is 80.0 m and the wet weight per unit length is 9.1 N/m.

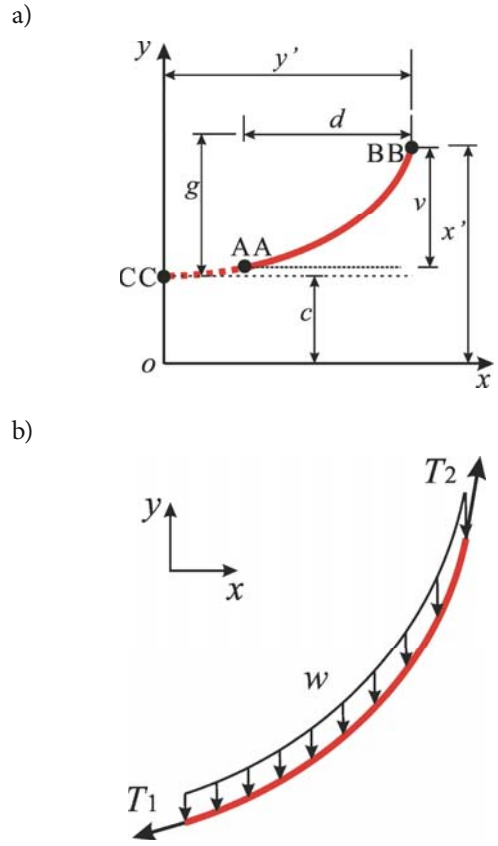

Fig. 6 Catenary curve: (a) the sketch; (b) the forces

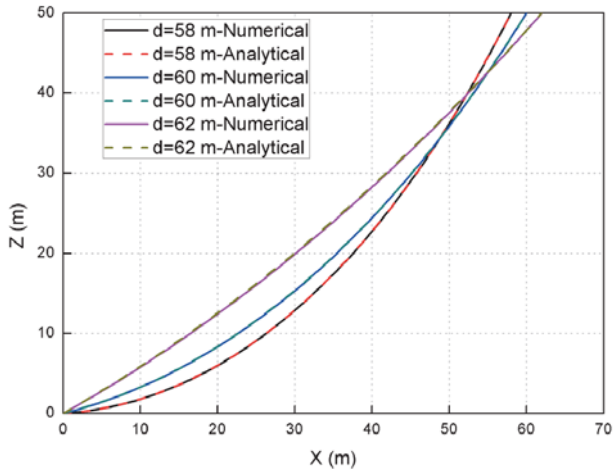

Fig. 7 Comparison of fiber rope profiles between the numerical simulations and analytical results

Fig. 7 shows the profiles of fiber rope with the variation of the horizontal distance d, which are calculated from the numerical simulations and analytical method. The results show a good agreement of the profile of fiber rope is achieved for different horizontal distances. In addition, the tension at the top end of fiber rope is listed in Table 1. It reveals that the static tension on suspended rope could be estimated accurately through the numerical simulations. Therefore, our proposed numerical model is available and appropriate to predict the configuration and static tension response of suspended rope.

Tab. 1 Top end tension on fiber rope for different horizontal distances

Horizontal distance (m)	Method	Tension (N)			Error (%)
		Horizontal	Vertical	Total	
58.0	Numerical	386.7	748.1	842.2	0.89
	Analytical	393.6	753.0	849.2	
60.0	Numerical	552.9	854.6	1017.8	0.86
	Analytical	555.2	863.6	1026.7	
62.0	Numerical	1296.3	1430.9	1930.7	3.47
	Analytical	1354.1	1472.0	2000.1	

DYNAMIC ANALYSIS

The dynamic behavior of suspended mooring line is validated by the experimental results by Chen et al. 2001 through the forced oscillation tests in this context. The mooring line is anchored at the bottom and a prescribed unidirectional harmonic motion is excited on the top end. The brief description of the process is given below.

The mooring line is composed of mooring chains with a spring inserted in the middle position. The water depth of 223.5 m was applied in tests and the main physical properties of mooring line are given in Table 2. And the in-plane regular oscillations at the top end with the amplitudes and periods listed in Table 3 were conducted in the numerical model. The amplitude ratio is defined as the ratio of the average of peak-to-peak line tension to the average of peak-to-peak top-end motion. Comparisons of the amplitude ratios with the variation of the frequency between the numerical simulations and experimental results in Chen et al. 2001 are shown in Fig. 8. It demonstrates that the numerical results are in a good agreement with the experimental results in the entire frequency range included in Table 3. This indicates that the

present numerical model is quite reasonable to predict the dynamic tension response of mooring line.

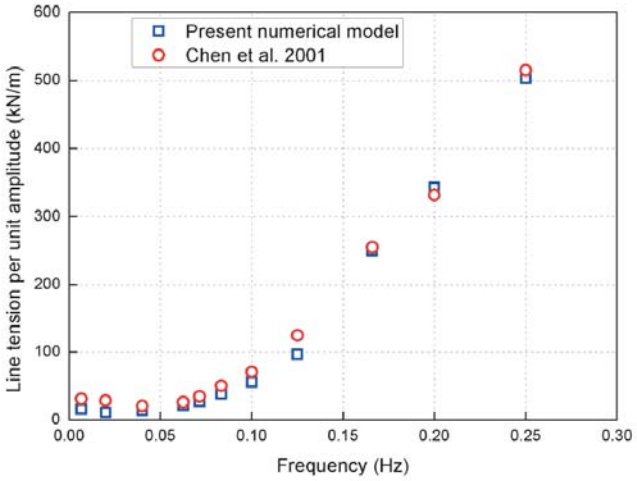

Fig. 8 Line tension per unit amplitude with the variation of the frequency in oscillation tests

Tab. 2 Properties of mooring line in physical tests (Chen et al. 2001)

Component	Item	Value
Chain	Nominal diameter (m)	0.2
	Chain length (m)	635
	Mass per unit length (kg/m)	834.1
	Elastic stiffness (kN)	2.98×10^7
	Hydrodynamic coefficient C_{Dt}	0.6
	Hydrodynamic coefficient C_{Dn}	3.2
	Hydrodynamic coefficient C_{Mt}	0.6
	Hydrodynamic coefficient C_{Mn}	2.8
Inserted spring	Position of the spring	In the middle
	Unstretched length (m)	48.8
	Elasticity (kN/m)	56.5
	Mass per unit length (kg/m)	1185.6
	Pretension (kN)	4453.7

Tab. 3 Harmonic oscillation parameters in physical tests (Chen et al. 2001)

No. of test	Amplitude (m)	Period (s)
1	0.9144	4.0
2	0.9144	5.0
3	0.9144	6.0
4	4.572	8.0
5	6.096	10.0
6	9.144	12.0
7	9.144	14.0
8	9.144	16.0
9	9.144	25.0
10	36.576	50.0
11	36.576	150.0

RESULTS AND DISCUSSION

Numerical simulations are conducted to investigate the structural response of mooring line with embedded chains: first, the effect of embedded chains on the response of mooring line is investigated by the proposed numerical model; second, the parameter sensitivity for mooring line with embedded chains is calculated in static and dynamic analysis; finally, the dynamic response of net cage system including the soil resistance is adopted to evaluate how much influence of embedded chains.

The mooring line is installed in 50 m water depth. In the numerical model, the mooring line is discretized into 50 elements and half of them are allocated to chains. And most of chains are assumed to be buried in soil. The wet unit weight of soil is 18.80 kN/m^3 to obtain the effective chain weight in soil (Degenkamp and Dutta 1989). The parameters of mooring line in the numerical simulations are tabulated in Table 4. The top end of mooring line is located at a depth of 5 m below the water surface level to be consistent with the parameters of anchor line for net cage system.

Tab. 4 Parameters of mooring line in the numerical simulations

Component	Parameter	Value
Suspended rope	Diameter (m)	0.091
	Density (kg/m^3)	953
	Material	PP
	Rope length (m)	57.6
	Elastic coefficient (MN)	3.52
	Initial pretension (kN)	138.1
Embedded chains	Diameter (m)	0.030
	Density (kg/m^3)	7850
	Material	Steel
	Chain length (m)	6.4
	Elastic coefficient (MN)	284.2
	Initial pretension (kN)	0.0

THE INFLUENCE OF EMBEDDED CHAINS ON THE RESPONSE OF MOORING LINE

Five cases are investigated to quantify the influence of embedded chains on the response of hybrid mooring line in static and dynamic analysis in this section. Fig. 9 shows the schematic diagram of Case 0, Case A, Case B, Case C and Case D. The reference case considering the effect of embedded chains is denoted as Case 0 and the anchor point is located at the point C in Fig. 9. And Case A, Case B, Case C and Case D represent different simplified positions (points A, B, C and D in Fig. 9 correspondingly) for the anchor point around the seabed level ignoring the impact of the soil resistance, where the lengths of mooring line are always 64.0 m. The effect of

embedded chains on static and dynamic response of mooring line is discussed as follows.

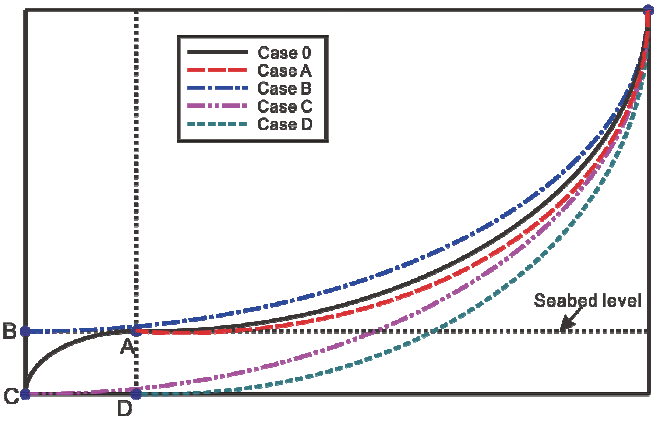

Fig. 9 Schematic diagram of Case 0, Case A, Case B, Case C and Case D

Static analysis

Tab. 5 Parameters of simplified fish cage system

Component	Parameter	Value
Outer circle	General diameter (m)	42.3
	Pipe diameter (m) Thickness (m)	0.625 0.0325
	Density (kg/m)	71.0
	Material	HDPE
Inner circle	General diameter (m)	39.8
	Pipe inner diameter (m) Thickness (m)	0.625 0.0325
	Density (kg/m)	71.0
	Material	HDPE
Bottom ring	Diameter (m) Pipe diameter (m) Density (kg/m) Material	39.8 0.15 25.3125 HDPE
Sinker	Diameter (m) Mass of each sinker (kg) Number	0.075 228.125 10
Rigid frame	Diameter (m) Thickness (m) Width (m) Height (m) Density (kg/m)	0.625 0.042 29.0 25.0 71.0
Mooring line	Anchor line length (m) Bridle line length (m) Buoy line length (m)	64.0 20.5 5.0

Figs. 10 and 11 show the profiles and static tension response of mooring line calculated from the numerical model in Case 0, Case A, Case B, Case C and Case D.

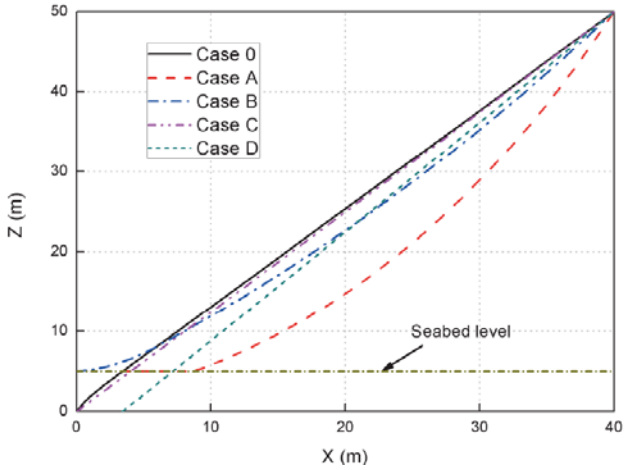

Fig. 10 Profiles of hybrid mooring line in five cases

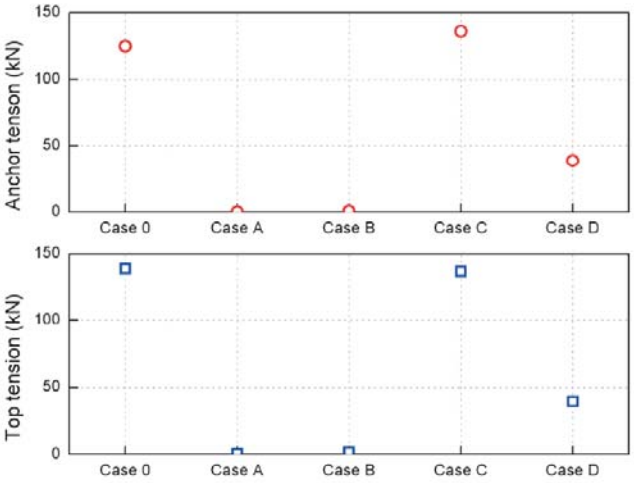

Fig. 11 Static tension force at the anchor point and the top end of mooring line

Obviously, the mooring line remains slack in Case A and Case B, and this leads to a small magnitude of tension force at both the anchor point and the top end. And the tension force at the anchor point and the top end of mooring line in Case D is significantly less than that in Case 0. Provided that the load acting on embedded anchors and offshore structures is equivalent to the tension force at the anchor point and the top end of mooring line, it is not reasonable by simplifying the mooring line as Case A, Case B and Case D to obtain the corresponding response of embedded anchors and offshore structures. Although the profile and the static tension in Case C are the nearest to those in Case 0, the difference of the tension at the anchor point between Case 0 and Case C could be up to 9.14%. This indicates that the load on embedded anchors predicted in Case C will be overestimated if neglecting embedded chains. It is noted that Case A, Case B, Case C and Case D fail to provide an acceptable result of the static response of mooring line regardless of the soil resistance.

Thus, the simulation of embedded chains in soil is beneficial to estimate the load on embedded anchors more accurately in design for practical engineering. If the static tension on the anchor point is estimated by Case C at the initial design phase, the safety factor of 1.09 should be included.

Dynamic analysis

The time history of dynamic tension response for hybrid mooring line is shown in Fig. 12, when the amplitude and period in harmonic oscillation are 4.0 m and 4.5 s.

a)

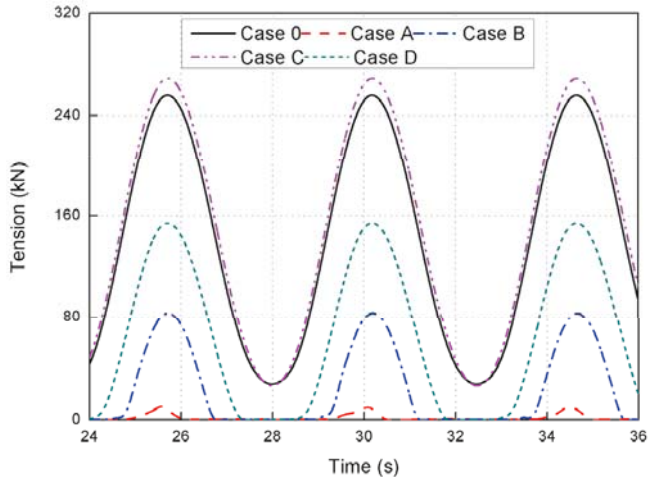

b)

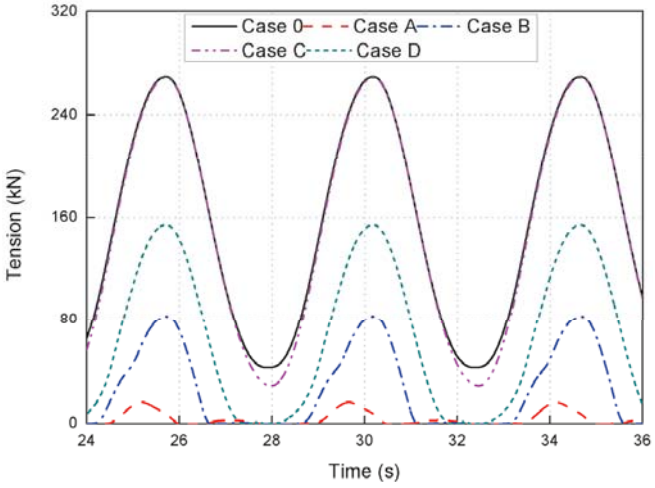

Fig. 12 Tension histories of mooring line at: (a) anchor point; (b) top end

The results reveal that the maximum tension at the top end of mooring line in Case 0 and Case C has little difference, whereas the maximum tension at the anchor point in Case C is overestimated. For Case A, Case B and Case D, it may be too dangerous to obtain the load acting on embedded anchors ignoring the effect of embedded chains. And the crest and trough of the tension history of mooring line in Case A, Case B and Case D is extremely asymmetrical. This indicates the slack of mooring line in Case A, Case B and Case D could induce the nonlinearity of tension response of mooring line. It can be concluded that Case A, Case B, Case C and Case D may result in an un-reasonable evaluation for the dynamic response of mooring line and embedded anchors. Therefore, the soil resistance on embedded chains is critical to the dynamic tension on mooring line and should be comprehensively investigated for the design of embedded anchors. At the initial design phase, the safety factor of 1.05 should be included to evaluate the maximum tension on the anchor point by Case C.

PARAMETER STUDY

In this section, the configuration and the tension response of mooring line with embedded chains are investigated to evaluate the effect of the variation of parameters, including initial pretension level of mooring line, soil shear strength gradient and the multipliers in soil resistance. The amplitude and period of harmonic oscillation in dynamic analysis are 4.0 m and 4.5 s.

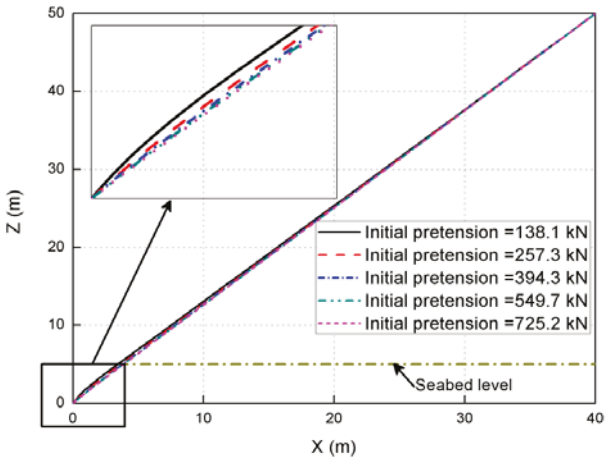

Fig. 13 Profiles of mooring line for different initial pretension levels

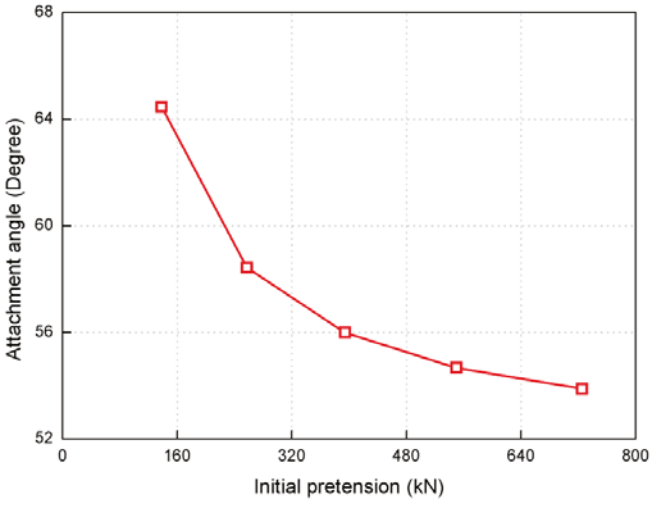

Fig. 14 Attachment angle of embedded chains with the variation of the initial pretension

Initial pretension level

The initial pretension level may affect the structural behavior of mooring line with embedded chains in static and dynamic analysis. The initial pretension investigated in this section involves the values of 138.1 kN, 257.3 kN, 394.3 kN, 549.7 kN and 725.2 kN for suspended rope. And the attachment angle θ (shown in Fig. 1) is defined as the angle of inclination of embedded chains at the anchor point, which is of vital importance to determine the mode failure and the embedded performance of embedded anchors. Fig. 13 shows the static configurations of mooring line and Fig. 14 presents the corresponding attachment angles of embedded chains with the variation of the initial pretension level. It can be inferred that the larger initial pretension of mooring line makes embedded chains tauter. As described in Fig. 14, the increase of initial pretension of mooring line results in the sharp decrease of the attachment angle of embedded chains substantially. This demonstrates that the initial pretension of mooring line may have a non-negligible influence on the attachment angle of embedded chains and may lead to a significant variation of the vertical tension on embedded anchors.

a)

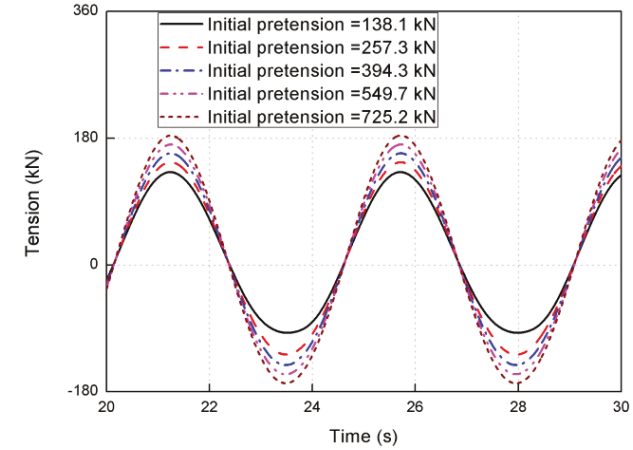

b)

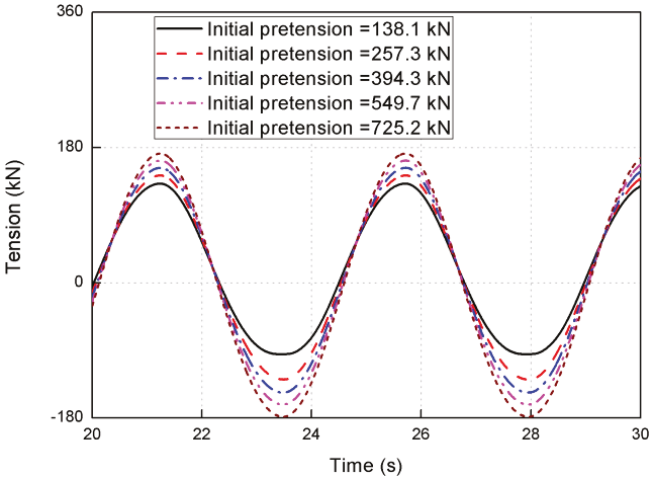

Fig. 15 Time history of mooring line tension at: (a) anchor point; (b) top end

Fig. 15 presents the time history of tension force on mooring line for different initial pretension levels, where the static tension at the anchor point and top end is subtracted correspondingly. The crest and trough of the tension history of mooring line becomes gradually symmetrical with the increase of the initial pretension. This indicates that the nonlinear effect of tension history of mooring line becomes weaker with a larger initial pretension due to the tauter embedded chains (shown in Fig. 13). And the tauter embedded chains the larger tension at the anchor point of mooring line. In addition, when the initial pretension of mooring line increases, the maximum tension force at the anchor point of mooring line has almost a linearly upward trend as seen from Fig. 15. Therefore, the initial pretension of mooring line is beneficial to make embedded chains tauter, and thus the mean offset of fish cage system could be limited in an acceptable range to meet the design requirement of mooring system. However, the load capacity of embedded anchors would increase and enhance the cost of embedded anchors. Thus it is crucial to select an appropriate value of initial pretension of mooring line to achieve a balance between the safety of net cage and the economic cost of embedded anchors in context of the safety of the offshore net cage system.

Soil shear strength gradient

Since the soil resistance in Eq. (4) is proportional to the soil shear strength in Eq. (5), it is of great importance to investigate the sensitivity of the structural response of mooring line in static and dynamic analysis with respect to the soil shear strength gradient. In this section, soil shear strength at the seabed level s_{u0}= 0.0 kPa is always used, whereas the soil shear strength gradient k changes with different hypothetical cases.

The soil shear strength gradient varies from 0.725 kPa/m to 3.625 kPa/m with a constant increment of 0.725 kPa/m, and the corresponding static and dynamic results of mooring line are shown in Fig. 16. The results indicate the profile and maximum tension force at the anchor point of mooring line is significantly sensitive to the variation of the soil shear strength gradient. With the decrease of the soil shear strength gradient, the embedded chains become gradually tightened. And the attachment angles of embedded chains are 57.8°, 64.5°, 70.6°, 76.5° and 82.4° for soil shear strength gradient from 0.725 kPa/m to 3.625 kPa/m. It is demonstrated that the mooring line development has great sensitivity to the soil shear strength gradient. Fig. 16b illustrates that the maximum tension at the top end of mooring line is more significant than that at the anchor point, especially for a large soil shear strength gradient. This may be a consequence of being the embedded part of mooring line supported by soil, while the un-embedded part is kept taut under a large tension. When the soil shear strength gradient increases, the maximum tension force at the anchor point of mooring line has a significant downward trend, while the maximum tension force at the top end has a slight upward trend. Different from a larger tension on the tauter embedded chains as mentioned above, the increase of the soil resistance results in the decrease of the tension at the anchor point of embedded chains on the basis

of the principle of the equilibrium of internal and external forces. The relative difference of the maximum tension at the anchor point of mooring line for the soil shear strength gradient between 0.725 kPa/m and 3.625 kPa/m could be up to 10.44%. This indicates that the soil shear strength gradient is dominant for the load carrying capacity of embedded anchors in the design. Thus the soil shear strength gradient should be determined carefully through the geological survey before the design of the fish farm for predicting the tensile capacity of embedded anchors and the mooring performance accurately.

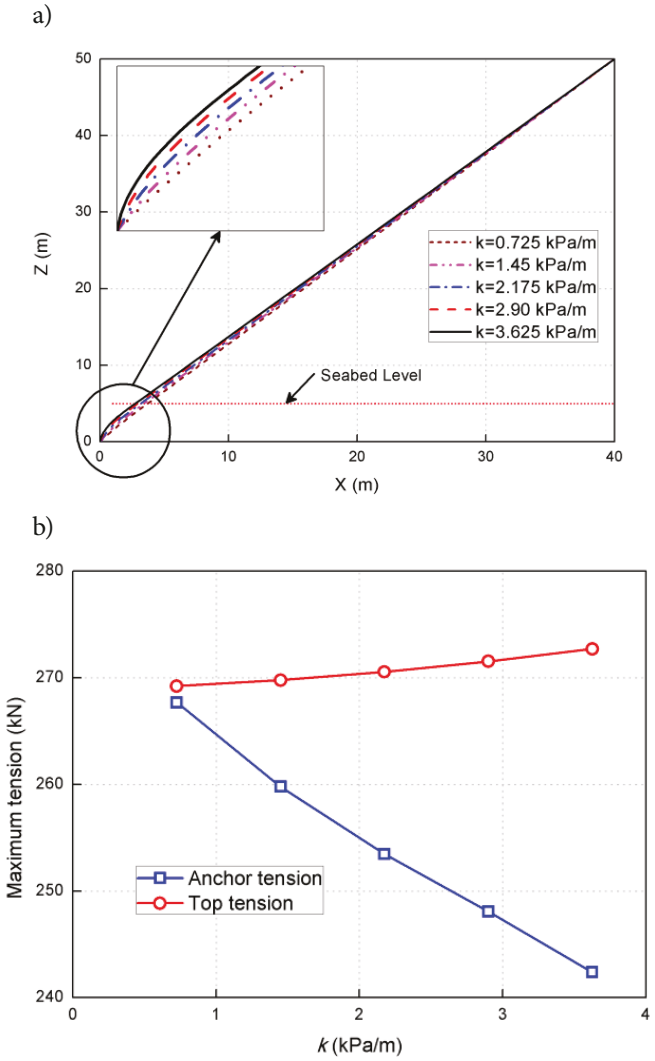

Fig. 16 Response results of mooring line: (a) profiles; (b) maximum tension force

Multipliers in soil resistance

Based on the principle of the equilibrium of internal and external forces, the variation of normal soil resistance for different multipliers may affect the mooring line development and the tension response of mooring line. The value of E_n is recommended as 1.0 and 2.5 for cables and chains, and the value of N_c rises from 5.1 at the seabed to 7.6 at a chain depth of 6d (d is the nominal diameter of embedded chains) (Degenkamp and Dutta 1989). In this section, the sensitivity of the static and dynamic response of mooring line to the variation of the product of E_n, N_c is investigated to evaluate the effect of normal soil resistance.

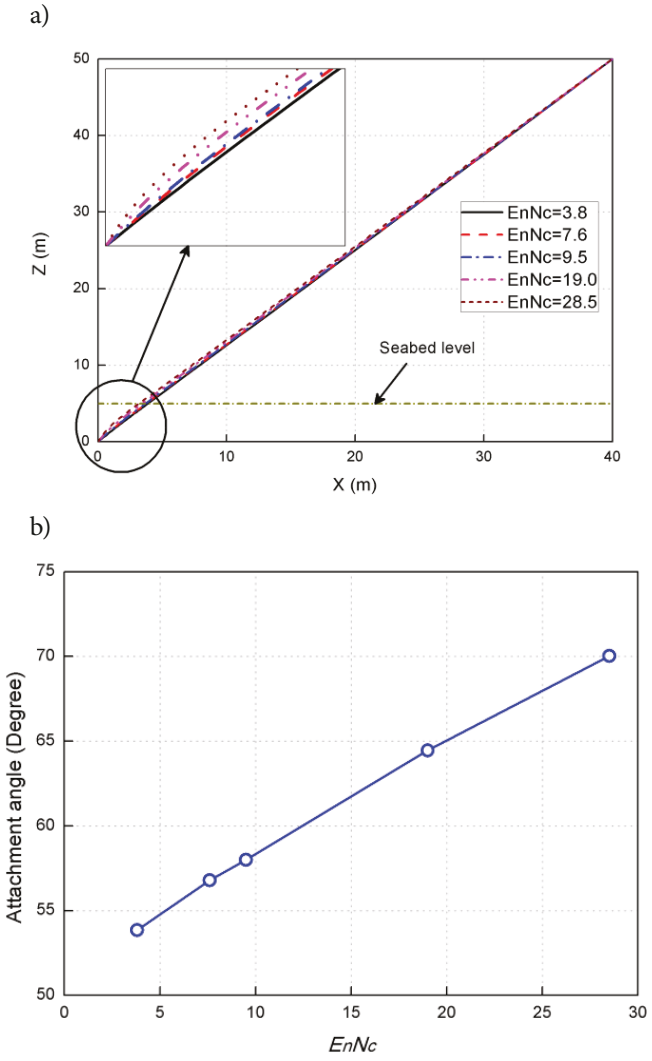

Fig. 17 Sensitivity to the value of $E_n \cdot N_c$: (a) mooring line profile; (b) attachment angle

Fig. 17 shows the configuration and the corresponding attachment angle of mooring line with the variation of the value of $E_n \cdot N_c$. The results demonstrate that the embedded chains supported by soil become slack apparently and the attachment angle of embedded chains increases approximately linearly with the increase of the value of $E_n \cdot N_c$. And Fig. 18 presents the tension response of mooring line for different values of $E_n \cdot N_c$. This indicates that there is no significant difference between the tension at both the anchor point and top end of mooring line for different normal soil resistance. However, the vertical component of the tension on embedded anchors may reach the allowable maximum, due to the large inclination angle at the anchor point of mooring line with increasing value of $E_n \cdot N_c$. This indicates that it is conservative to consider the effect of embedded chains with the large value of $E_n \cdot N_c$ to obtain the vertical component of the tension on embedded anchors. Thus, the impact of normal soil resistance is significant on the mooring line development and the

vertical component of the tension on embedded anchors and should be included during the design phase of mooring system.

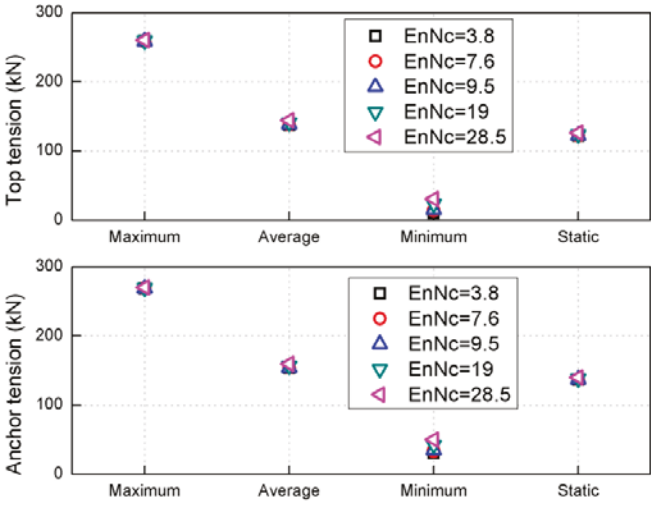

Fig. 18 Sensitivity of the tension on mooring line to the value of $E_n \cdot N_c$

DYNAMIC ANALYSIS OF NET CAGE SYSTEM WITH EMBEDDED CHAINS

In this section, a full dynamic analysis of mooring system for net cage in the open sea is conducted and the moored fish cage system was installed in 50 m water depth. Following previous works (Xu et al. 2014), this study adopted the self-developed numerical model based on the lumped-mass method and rigid body kinematics principle to obtain the dynamic response of net cage and mooring system. The net cage and mooring system is composed of a gravity cage and a single-point mooring system with a frontal rigid frame, as shown in Fig. 19. The fish cage consists of float collar, net pen, bottom ring and sinkers. The cage net is made of PE with a mass density of 953 kg/m^3. There are 90 meshes in the circumferential direction and 12 meshes in the depth direction. The net is knotless, with a mesh size of 29.25 mm and a twine thickness of 1.80 mm. When mounted as diamond meshes, the net forms an open vertical cylinder with a diameter of 39.8 m and a height of 22.5 m. The anchor line is composed of embedded chains and fiber rope and the main properties have been listed in Table 4. The detailed parameters of fish cage and mooring system are given in Table 5.

In this section, Case 0 and Case C mentioned in Section 4.1 are adopted as the anchor line of net cage system (see Fig. 19b) and the cases are correspondingly denoted as Case S0 and Case SC to evaluate the effect of embedded chains. Here the wave-frequency excitation with the wave height of 4.0 m and period of 4.5 s is employed for a certain probability of occurrence at Bohai bay area in one year according to Global Wave Statistics Online (www.globalwavestatistics.com). Fig.20 provides the maximum tension force on mooring system in single-cage system in Case S0 and Case SC, including bridle lines, anchor lines and buoy line. Anchor-1 and Anchor-2 are described as the pad-eye point and the top end of anchor line.

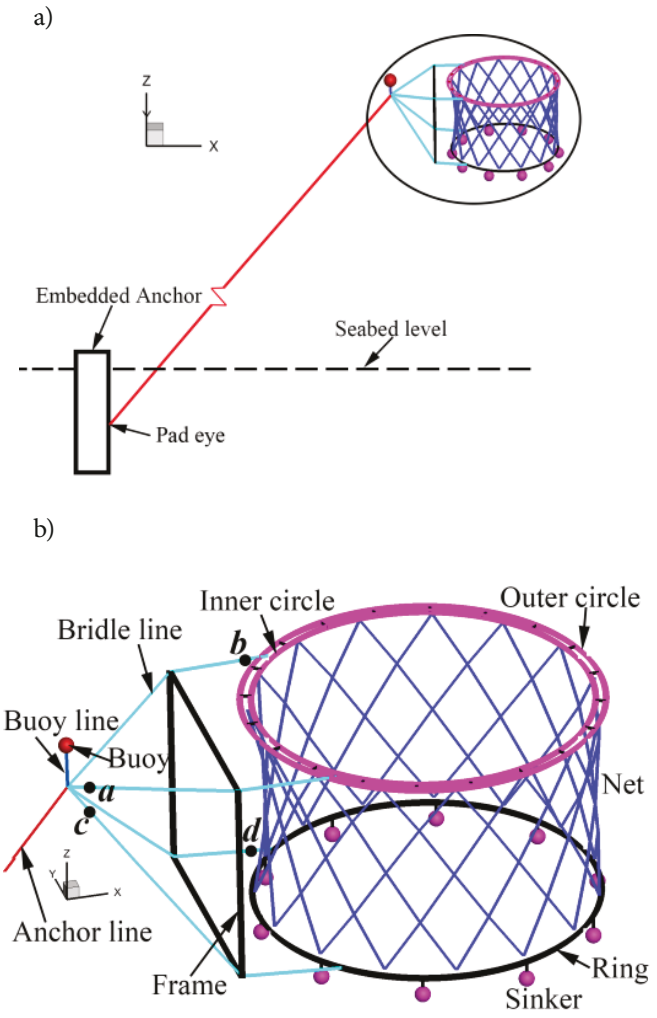

Fig. 19 Schematic of: (a) open sea fish farm system; (b) net cage system`

As shown in Fig. 20, the soil resistance on embedded chains has a negligible effect on the maximum tension on bridle lines and buoy line. And for net cage, the maximum volume reduction factor in Case S0 and Case SC are 7.15% and 7.14%. The insignificant difference of the dynamic response of net cage between considering and neglecting the effect of embedded chains may be attributed to the insignificant variation of the tension response at the top end of anchor line (see Fig. 20). Due to the insignificant force transmission from the anchor line, the dynamic response of the upper structure is almost uninfluenced by embedded chains. However, the difference of maximum tension at the pad-eye point of anchor line between Case S0 and Case SC is 8.19%. And the tension response at the pad-eye point in Case S0 is significantly less than that in Case SC, consistent with the results in Section 4.1. The results indicate that the existence of soil resistance should not be neglected for estimating the load acting on embedded anchors precisely.

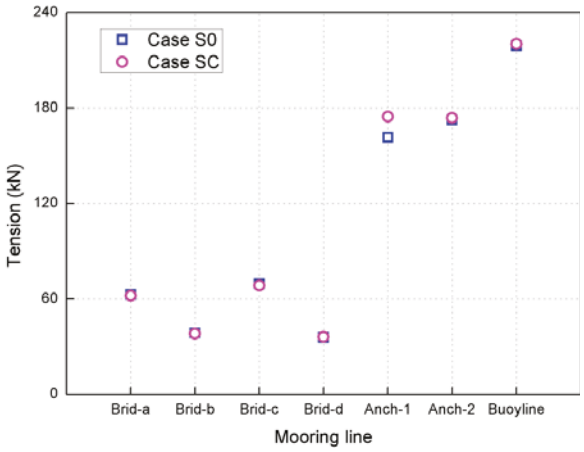

Fig. 20 Maximum tension on mooring system of Case S0 and Case SC

In addition, the dynamic response at the pad-eye point of anchor line for multi-cage system is investigated considering the anchor line with and without embedded chains as Case 0 and Case C. And the cases for the double-cage system and four-cage system (shown in Fig. 21) with anchor line in Case 0 and Case C are denoted as Case D0, Case DC and Case F0, Case FC, respectively.

a)

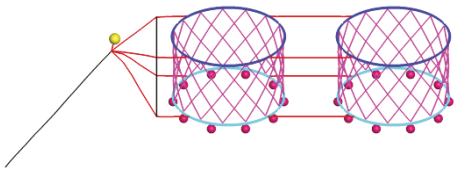

b)

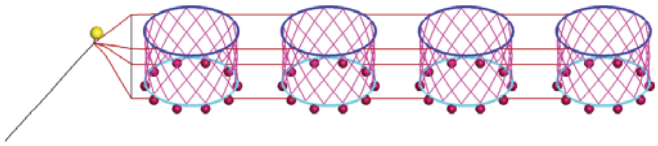

Fig. 21 Schematic of: (a) double-cage system; (b) four-cage system

Fig. 22 shows the tension histories at the pad-eye point of anchor line in Case S0, Case SC, Case D0, Case DC, Case F0 and Case FC. The maximum tension on anchor line for multi-cage system is more remarkable than that for single-cage system. The relative difference of the maximum tension on anchor line between Case D0 and Case DC is 5.62%, while the relative difference of the maximum tension between Case F0 and Case FC is 4.02%. The decrease of the relative difference of tension response may be attributed to the decreasing proportion of the soil resistance to the external load with the growth of the scale of net cage system. And the interaction of soil and embedded anchors would be dominant for the safety of embedded anchors and the large-scale system in service.

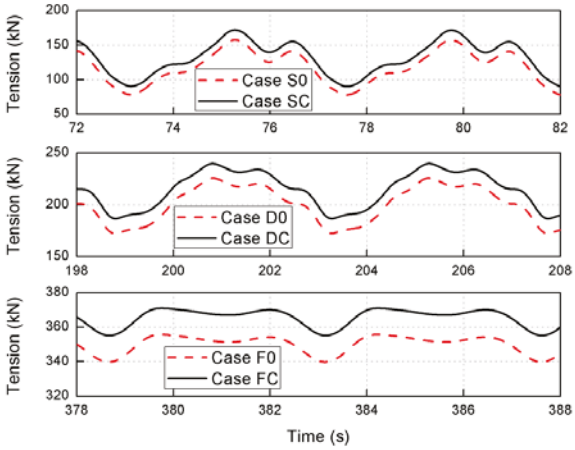

Fig. 22 Tension histories of anchor line at the anchor point

While the mooring line undergoes cyclic environmental loads in service, the embedded chains will have a cyclic motion due to the top end motion and cause the degradation of the soil shear strength around embedded anchors. And the embedded chains and seabed interaction will induce the soil trenching near embedded anchors as the soil experiences the cycles of loading and unloading. However, it can be seen from Fig. 22 that the load on embedded anchors would be more significant after the trenching phenomenon appears. Meanwhile, the surrounding soil of embedded anchors will be remolded and may decrease the holding capacity of embedded anchors. As a consequence, the embedded anchors would move and may be even pulled out, which is undesirable during the operation of offshore structures. Thus it is essential to include embedded chains into anchor line and propose a full coupled model to estimate the interaction among mooring system, embedded anchors, soil and offshore net cage system in the future work.

CONCLUSIONS

A numerical model for hybrid mooring line considering embedded chains in soil is developed. The proposed numerical model was validated by analytical formulations in static analysis and experimental results in dynamic analysis, respectively. The results indicate that our numerical model is available to predict the structural response of mooring line with embedded chains. Several conclusions can be drawn as follows:

The simplified cases of mooring line ignoring the effect of embedded chains, including Case A, Case B, Case C and Case D, would result in an un-reasonable evaluation for the static and dynamic response of mooring line and embedded anchors, and it is essential to select an appropriate safety

factor using the simplified model at the initial design stage. In parameter sensitivity study, initial pretension of suspended rope and the soil shear strength gradient have a significant effect on mooring line development and the load acting on embedded anchors. For single-cage system, the difference of the maximum tension at the pad-eye point of anchor line between Case S0 and Case SC could be up to 8.19%. And the corresponding difference for double-cage and four-cage system is 5.62% and 4.02%.The reduction of the impact of embedded chains may be attributed to the smaller proportion of the soil resistance to the external load for the larger-scale net cage system. However, the interaction of soil and embedded anchors for the multi-cage system may increase, and the trenching phenomenon may appear resulting in the decrease of the soil shear strength and capacity of embedded anchors. In the future work, the interaction with embedded chains, soil and embedded anchors for net cage system in the open sea and how to improve the safety condition deserves to be further studied.

ACKNOWLEDGEMENTS

This work was financially supported by National Key R&D Program of China (2017YFC1404200), the National Natural Science Foundation (NSFC) Projects No. 51409037, and the Fundamental Research Funds for the Central Universities No. DUT18LK41.

APPENDIX A ANALYTICAL FORM FOR STATIC RESPONSE OF EMBEDDED CHAINS

According to Vivatrat et al. 1982, the differential equations of embedded chains are

$$\begin{aligned} \frac{dT}{dl} &= F + W \cdot \sin\theta \\ T \cdot \frac{d\theta}{dl} &= -Q + W \cdot \cos\theta \end{aligned} \quad \text{(A. 1)}$$

where W is the wet weight per unit length of chains; θ is the angle from the chains to the horizontal axis; T is the chain tension; l is the distance along the chains, starting at the anchor point; F and Q are the normal and tangential components of soil resistance on chains, respectively. Considering the small attachment angle assumption and ignoring the chain weight (referring to Neubecker and Randolph 1995), the analytical expression of the profile for embedded chains can be written as,

$$dx^* = -\frac{dz^*}{\sqrt{\theta_o^2 + \frac{2}{T^*}\cdot(z^*)^2}} \quad \text{(A. 2)}$$

where x^* and z^* are the horizontal and vertical coordinates normalized by the attachment depth D; θ_o is the chain angle at the seabed; T^* is the non-dimensional tension at the attachment point, $T^* = \frac{T_a}{DQ}$. Thus the profile can be expressed as,

$$\sqrt{2/T^*}\cdot x^* = \ln\left[\left(1+\sqrt{1+T^*\cdot\theta_o^2/2}\right)/\left(z^*+\sqrt{(z^*)^2+T^*\cdot\theta_o^2/2}\right)\right] \quad \text{(A. 3)}$$

APPENDIX B ANALYTICAL FORM FOR STATIC RESPONSE OF CATENARY CURVE

The global coordinate system and the sketch of catenary curve are shown in Fig. 6a. Points AA, BB and CC represent the anchor point, the top end and the virtual sag point, respectively. According to the derivation in Cella 1999, the formulas are shown as follows,

$$l = c\cdot\left(\sinh\left(\operatorname{atanh}\left(\frac{v}{l}\right)+\frac{d}{2c}\right)-\sinh\left(\operatorname{atanh}\left(\frac{v}{l}\right)-\frac{d}{2c}\right)\right) \quad \text{(B. 1)}$$

$$\frac{x'}{c} = \operatorname{atanh}\left(\frac{v}{l}\right)+\frac{d}{2c} \quad \text{(B. 2)}$$

$$y' = c+g = c\cdot\cosh\left(\frac{x'}{c}\right) \quad \text{(B. 3)}$$

where d is the horizontal distance between the top end and the anchor point; v is the vertical distance between the top end and the anchor point; l is the length of catenary curve; g is the distance between the top end and the virtual sag point of catenary curve; x' is the abscissa value of the top end in the global coordinate system; y' is the ordinate value of the top end in the global coordinate system; c is the ordinate value of the virtual sag point of catenary curve in the global coordinate system; sinh(·) and cosh(·) are the hyperbolic sine and cosine functions; atanh(·) is the arc-hyperbolic tangent function.

In this study, the variables v, d and l in Fig. 6a are known a priori. From Eq. (B. 1), the parameter c can be obtained by Newton-Raphson method. Subtracting c into Eq. (B. 2), the x' is calculated. Then the variable g is yielded by Eq. (B. 3). Therefore, the profile of the catenary curve can be calculated by,

$$y = c\cdot\cosh\left(\frac{x+x'-d}{c}\right)-(c+g-v) \quad \text{(B. 4)}$$

where x and y is the abscissa and ordinate values of the top end in the local coordinate system, respectively. The origin of the local coordinate system is located at the anchor point. The horizontal and the vertical components of the tension on catenary curve at the top end are

$$\begin{aligned} T_x &= w\cdot c \\ T_y &= w\cdot c\cdot\sinh\left(\frac{x'}{c}\right) \end{aligned} \quad \text{(B. 5)}$$

where w is the wet weight per unit length of catenary curve. Thus the total tension on catenary curve at the top end is

$$T = w\cdot c\cdot\cosh\left(\frac{x'}{c}\right) \quad \text{(B. 6)}$$

REFERENCES

1. Andersen, K.H., Murff, J.D., Randolph, M., Clukey, E.C., Erbrich, C.T., Jostad, H.P., Hansen, B., Aubeny, C.P., Sharma, P., Supachawarote, C., 2005. Suction anchors for deepwater applications. In: Proceedings of the International Symposium on Frontiers in Offshore Geotechnics, 3-30.

2. Cella, P., 1999. Methodology for exact solution of catenary. Journal of Structural Engineering, 125(12): 1451-1453.

3. Chen, X.H., Zhang, J., Johnson, P., Irani, M., 2001. Dynamic analysis of mooring lines with inserted springs. Applied Ocean Research 23, 277-284.

4. Cheng, M.Y., Cao, M.T., Tran, D.H, 2014. A hybrid fuzzy inference model based on RBFNN and artificial bee colony for predicting the uplift capacity of suction caissons. Automation in Construction 41, 60-69.

5. Choi, Y., Kim, B., Kwon, O., Youn, H., 2014. Horizontal pullout capacity of steel chain embedded in sand. Advances in Soil Dynamics and Foundation Engineering GSP, 240, 500-508.

6. Choo, Y.I., Casarella, M.J., 1971. Hydrodynamic resistance of towed cables. Journal of Hydronautics, 126-131.

7. DeCew, J., Tsukrov, I., Risso, A., Swift, M.R., Celikkol, B., 2010. Modeling of dynamic behavior of a single-point moored submersible fish cage under currents. Aquacultural Engineering 43(2), 38-45.

8. Degenkamp, G., Dutta,A., 1989. Soil resistances to embedded anchor chain in soft clay. Journal of Geotechnical Engineering 115(10), 1420-1438.

9. Gault, J.A., Cox, W.R., 1974. Method for predicting geometry and load distribution in an anchor chain from a single point mooring buoy to a buried anchorage. In: Proceedings of 6th Annual Offshore Technology Conference. Houston, Texas, USA, 309-318.

10. Guo, Z., Wang, L.Z., Yuan, F., 2016. Quasi-static analysis of the multi-component mooring line for deeply embedded anchors. Journal of Offshore Mechanics and Arctic Engineering, 138(1), paper No: OMAE-11-1097.

11. Hall, M., Goupee, A., 2015. Validation of a lumped-mass mooring line model with DeepCwind semisubmersible model test data. Ocean Engineering 104, 590-603.

12. Huang, X.H., Guo, G.X., Tao, Q.Y., Hu, Y., Liu, H.Y., Wang, S.M., Hao, S.H., 2016. Numerical simulation of deformations and forces of a floating fish cage collar in waves. Aquacultural Engineering 74, 111-119.

13. Huang, C.C., Tang, H.H., Liu, J.Y., 2006. Dynamic analysis of net cage structures for marine aquaculture: Numerical simulation and model testing. Aquacultural Engineering 35(3), 258-270.

14. Huang, C.C., Tang, H.J., Wang, B.S., 2010. Numerical modeling for an In Situ single-point-mooring cage system. IEEE Journal of Oceanic Engineering 35(3), 565-573.

15. Kapetsky, J.M., Aguilar-Manjarrez, J., Jenness, J., 2013. A global assessment pf potential for offshore mariculture development from a spatial perspective. FAO Fisheries and Aquaculture Technical Paper No. 549. Rome, FAO. 181 pp.

16. Kim, T., Lee, J., Fredriksson, D.W., DeCew, J., Drach, A., Moon, K., 2014. Engineering analysis of a submersible abalone aquaculture cage system for deployment in exposed marine environments. Aquacultural Engineering 63, 72-88.

17. Liu, H.X., Liu, C.L., Zhao, Y.B., Wang, C., 2014. Comparative study of reverse catenary properties of the installation line for drag anchors. Applied Ocean Research 48, 42-54.

18. Masciola, M.D., Nahon, M., Driscoll, F.R., 2011. Static analysis of the lumped mass cable model using a shooting algorithm. ASCE Journal of Waterway, Port, Coastal, and Ocean Engineering

19. Neubecker, S.R., Randolph, M.F., 1995. Profile and frictional capacity of embedded anchor chains. Journal of Geotechnical Engineering 121(11), 797-803.

20. O'Loughlin, C., White, D., Stanier, S., 2015. Novel anchoring solutions for FLNG-Opportunities driven by scale. In: Proceedings of the 47th Annual Offshore Technology Conference, Houston, Texas, USA, OTC-26032-MS.

21. Rocha, M., Schnaid, F., Rocha, C., Amaral, C., 2016. Inverse catenary load attenuation along embedded ground chain of mooring lines. Ocean Engineering 122, 215-226.

22. Shainee, M., DeCew, J., Leira, B.J., Ellingsen, H., Fredheim, A., 2013. Numerical simulation of a self-submersible SPM cage system in regular waves with following currents. Aquacultural Engineering 54, 29-37.

23. Skempton, A.W., 1951. The bearing capacity of clays. Building Research Congress, Division 1, Part 3, London, 180-189.

24. Surendran, S., Goutam, M., 2009. Reduction in the dynamic amplitudes of moored cable systems. Ships and Offshore Structures 4(2), 145-163.

25. Tang, H.J., Huang, C.C., Chen, W.M., 2011. Dynamics of dual pontoon floating structure for cage aquaculture in a two-dimensional numerical wave tank. Journal of Fluids

and Structures 27, 918-936.

26. Vivatrat, V., Valent, P.J., Ponterio, A.A., 1982. The influence of chain friction on anchor pile design. In: Proceedings of the 14th Annual Offshore Technology Conference, Houston, Texas, USA, 153-163.

27. Wang, L.Z., Guo, Z.,Yuan, F., 2010a. Quasi-static three dimensional analysis of suction anchor mooring system. Ocean Engineering 37, 1127-1138.

28. Wang, L.Z., Guo, Z.,Yuan, F., 2010b. Three-dimensional interaction between anchor chain and seabed. Applied Ocean Research 32, 404-413.

29. Xiong, L.Z., Yang, J.M., Zhao, W.H., 2016. Dynamic of a taut mooring line accounting for the embedded anchor chains. Ocean Engineering 121, 403-413.

30. Xu, T.J., 2014. Hydrodynamics of net cage group in the open sea. Doctoral Thesis. Dalian University of Technology.

31. Xu, T.J., Dong, G.H., Li, Y.C., Guo, W.J., 2014. Numerical study of a self-submersible single-point mooring gravity cage in combined wave-current flow. Applied Ocean Research 48, 66-79.

32. Xu, T.J., Zhao, Y.P., Dong, G.H., Gui, F.K., 2013. Analysis of hydrodynamic behavior of a submerisible net cage and mooring system in waves and current. Applied Ocean Research 42, 155-167.

33. Yen, B.C., Tofani, G.D., 1984. Soil resistance to stud link chain. In: Proceedings of 16th Annual Offshore Technology Conference, Houston, Texas, USA, OTC 4769, 1-10.

34. Zhao, Y.P., Bi, C.W., Chen, C.P., Li, Y.C., Dong, G.H., 2015. Experimental study on flow velocity and mooring loads for multiple net cages in steady current. Aquacultural Engineering 67, 24-31.

CONTACT WITH THE AUTHORS

Tiao-Jian Xu
e-mail:*1533191728@qq.com*

State Key Laboratory of Coastal and Offshore Engineering
Dalian University of Technology
No.2 Linggong Road
116024 Dalian City
CHINA